2017 American Control Conference
Sheraton Seattle Hotel
May 24–26, 2017, Seattle, USA

Robust Control of a Powered Transfemoral Prosthesis Device with Experimental Verification*

Vahid Azimi[1†], Tony Shu[2], Huihua Zhao[2], Eric Ambrose[2], Aaron D. Ames[3], Dan Simon[1]

***Abstract*— This paper presents, compares, and experimentally implements two robust model-based controllers for transfemoral prosthetic walking: the robust passivity (RP) controller and the robust sliding mode (RS) controller. These findings constitute the first steps toward using model-based controllers for prosthetic devices as an alternative to commonly-used variable impedance and proportional-derivative (PD) control methods. The model upon which the controllers are based is a 5-link planar hybrid system (both continuous and discrete behaviors) with point feet, to represent a transfemoral amputee's body and limbs. A desired walking trajectory is generated through the framework of human-inspired control by solving an optimization problem. Smooth humanlike gait is achieved by combining model information with a desired trajectory. The stability of both controllers is proven for continuous dynamics within the framework of the Lyapunov stability theorem. Simulations show the proposed controllers are capable of meeting specific performance requirements regarding trajectory tracking of the prosthetic knee and convergence to a stable periodic orbit while walking on flat ground. Finally, both RP and RS controllers are experimentally implemented on AMPRO3 (the third iteration of Advanced Mechanical Prosthesis), a custom self-contained powered transfemoral prosthesis. Results show that both controllers provide humanlike walking and accurate tracking performance for a healthy human subject utilizing a transfemoral prosthesis.**

I. INTRODUCTION

The number of transfemoral amputees in the United States is estimated at around 222,000 [1]. Amputees can use prosthetic legs in an attempt to restore a normal walking gait. Actuated active prostheses can provide more stable and natural walking compared with passive and semi-active prostheses, while simultaneously requiring less force and energy from the user [2]. The significant number of transfemoral amputees and greater efficiency of active prostheses motivate researchers to work on the design and control of powered lower-limb prostheses [3], [4].

Variable impedance control is one of the most popular approaches to control prostheses due to its model independence [5]–[7]. However, impedance control lacks optimality and robustness due to several shortcomings: tedious impedance parameter tuning (unique to each specific amputee subject), difficulties in detecting the sub-phases during a single step, lack of feedback, and passiveness [5], [8]–[10]. There have been several attempts to address the limitations of ordinary impedance control [11], [12].

However, the aforementioned controllers are model-independent, and lack mathematical proof of stability and robustness in the presence of system uncertainties, unmodeled dynamics, and disturbances. This motivates the design of robust model-based controllers for prosthetic devices, formally guaranteeing the convergence of system error trajectories and quantitatively establishing robustness to known perturbations. Importantly, such control methods need not be concerned with correct step cycle division (for switching between sub-phases) and tedious parameter tuning. In the context of this motivation, several works have been presented on bipedal robots and rehabilitation robots [13]–[15].

The main contributions of this paper are twofold: (i) Quantified tracking performance and convergence to a stable limit periodic orbit for two model-based robust controllers in simulated prosthetic walking, and (ii) Experimental verification of both controllers on the powered transfemoral prosthesis AMPRO3 with a healthy human subject.

To begin, an active transfemoral prosthesis is modeled and interfaced with a general amputee model to build a point prosthetic foot 5-link planar model as a hybrid [16] human-prosthesis system. Using able-bodied reference trajectories, an optimal smooth humanlike gait is found by solving an optimization problem. For the hybrid system and corresponding optimal gait, two different model-based robust controllers, RS and RP, are designed. The proposed controllers are designed with the aim of achieving robustness to parametric uncertainties, unmodeled dynamics, and disturbances of the human-prosthesis system while providing good tracking. The stability of the proposed controllers is proven for continuous prosthesis system dynamics.

The proposed controllers are first verified in simulation for the human-prosthesis system and then implemented experimentally on AMPRO3 with a human test subject. Simulation and experimental results illustrate that both proposed controllers provide convincing tracking performance, stability, and reasonable prosthesis knee torque values emulating humanlike walking.

The paper is organized as follows. Section II describes the combined human-prosthesis system and gives an overview of human-inspired outputs and humanlike gait. Section III presents the robust controllers' structures and provides their stability analysis. Section IV presents simulation results of the proposed systems. Section V presents experimental results of both proposed controllers on AMPRO3. Section VI presents concluding remarks and future work.

*This work is supported by NSF Award NRI-1526519 and NSF Grant 1344954. This research was approved by the George Institute of Technology Institutional Review Board as IRB2014-0382F for testing with humans.

[1] Cleveland State University, Cleveland, OH, USA
[2] Georgia Institute of Technology, Atlanta, GA, USA
[3] California Institute of Technology, Pasadena, CA, USA
[†] Corresponding author: v.azimi@csuohio.edu

II. HUMAN-PROSTHESIS COMBINED SYSTEM

In this section, a five-link planar model with a point prosthetic foot (one torso, two thighs, and two calves) is presented as a combined system, which includes a combined human model and transfemoral prosthetic model as shown in Fig. 1a [11].

A. Prosthesis Model

The prosthetic device (the red portion in Fig. 1a) is modeled as an active transfemoral prosthesis with prismatic-prismatic-revolute-revolute (PPRR) joint structure as illustrated in Fig. 1b. The prosthesis is attached to the amputee at P_a (the socket adapter) shown in Fig. 1a. The world frame for the prosthesis system is represented as $O_o = \{x_o, y_o, z_o\}$. This prosthetic leg model has four degrees of freedom: horizontal and vertical displacements of the attach point P_a, thigh angle, and knee angle. The prosthetic ankle is assumed to be underactuated while the human side remains actuated at the ankle; the combined model can be considered as a two-domain hybrid asymmetric human-prosthesis system with one domain for human stance and the other for prosthetic stance.

The equations of motion of the prosthetic leg shown in Fig. 1b are derived using the Euler-Lagrange formula:

$$M_p(q_p)\ddot{q}_p + C_p(q_p, \dot{q}_p)\dot{q}_p + g_p(q_p) = u_p \qquad (1)$$

where $q_p = (q_{p1}, q_{p2}, q_{p3}, q_{p4})^T$ represents the vector of generalized joint displacements of the prosthetic device (q_{p1} and q_{p2} are the horizontal and vertical displacement of the attach point P_a respectively, and q_{p3} and q_{p4} are thigh and knee angles respectively); $M_p \in \Re^{4\times4}$, $C_p \in \Re^{4\times4}$, and $g_p \in \Re^{4\times1}$ are the inertia matrix, Coriolis and centripetal matrix, and gravity vector respectively; u_p is the prosthesis control signal comprising horizontal and vertical forces at the hip and active control torques at the thigh and knee.

B. Hybrid Model

Because the combined system has both continuous and discrete behaviors (instantaneous velocity changes upon impact), the human-prosthesis bipedal structure can be considered a hybrid system [16] with configuration space Q_R in local coordinates $q_c = (q_{sf}, q_{sk}, q_{sh}, q_{nsh}, q_{nsk})^T$ and world frame $O_{co} = \{x_{co}, y_{co}, z_{co}\}$, illustrated in Fig. 1a. Using the Euler-Lagrange formula, the equations of motion of the bipedal continuous dynamics [12] are given as

$$M_c(q_c)\ddot{q}_c + C_c(q_c, \dot{q}_c)\dot{q}_c + g_c(q_c) = Bu_c \qquad (2)$$

where $M_c \in \Re^{5\times5}$ is the inertia matrix; $C_c \in \Re^{5\times5}$ is the Coriolis and centripetal matrix; $g_c \in \Re^{5\times1}$ is the gravity vector; $B \in \Re^{5\times5}$ is the torque map with underactuated prosthesis side and actuated human side; u_c is the vector of torque inputs.

To emulate humanlike walking, actual combined system outputs y_a must converge to desired (reference) human outputs y_d, where actual outputs y_a are comprised of forward hip velocity, knee angles, non-stance slope, and torso angle [12], [17]. An optimal smooth humanlike gait (i.e., desired human outputs y_d) is attained by solving an optimization problem composed of able-bodied reference trajectories along with partial hybrid zero dynamics (PHZD) constraints and the canonical walking function (CWF) [17]. Desired joint angles and angular velocities of the combined system (q_c^d) are calculated using the PHZD reconstruction procedure [17].

C. Problem Statement

The scope of this paper includes control of the prosthetic knee joint shown in Fig. 1a using the two proposed robust controllers introduced in Section III. These controllers receive input $S_c = \{q_c, q_c^d\}$ and hip information from the combined system. Using a linear transformation, the set $S_p = \{q_p, q_p^d\}$ is generated from S_c, where q_p^d is the desired trajectory for q_p. The controllers use S_p to generate prosthetic knee torque during both swing and stance phases, allowing the combined human-prosthesis system to emulate humanlike walking, i.e., $q_p \to q_p^d \Rightarrow q_c \to q_c^d \Rightarrow y_a \to y_d$ with bounded tracking error trajectories.

Since body coordinates are defined based on stance and non-stance phases, the fourth element of u_p is replaced by the second element of u_c when the prosthesis device is the stance leg, and likewise, the fourth element of u_p is replaced by the fifth element of u_c when the prosthesis is the non-stance leg (the first three elements of the u_p are dummy and not used). In this manner, the prosthesis control signal remains correctly defined during stance and non-stance phases. Our controllers use only body coordinates and able-bodied reference trajectories of the combined system, without any dynamic information of the healthy body, to generate prosthetic knee torque, which allows the combined human-prosthesis system to emulate humanlike walking. This implies that the proposed RS and RP controllers are robust not only against parameter uncertainties and unmodeled dynamics of the prosthesis, but also for different amputee subjects.

III. ROBUST PROSTHESIS CONTROLLERS

This section defines two different model-based robust controllers to control the prosthesis device (i.e., prosthetic knee joint, where prosthetic ankle is underactuated), simultaneously considering the shortcomings of traditional impedance control and providing a robust and stable control structure for prosthetic walking. As both controllers are model-based,

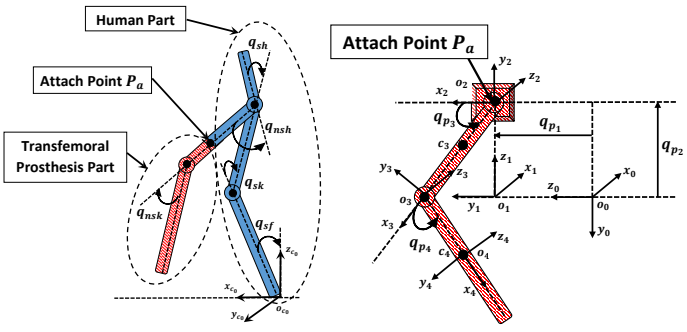

Fig. 1: (a) Combined human-prosthesis system, (b) Transfemoral prosthesis system

the prosthesis model depicted in Fig. 1b is used to control the prosthetic knee joint (red part) in Fig. 1a. To control the other joints and obtain stable and humanlike walking, a feedback linearization human-inspired controller is used to exponentially drive the actual outputs of the system to the desired ones [17].

A. Robust Sliding Mode Controller (RS)

An error vector s and signal vector v, which are n-element vectors, are defined as [18]

$$\begin{aligned} s &= \dot{e} + \lambda e \qquad v = \dot{q}_p^d - \lambda e \\ e &= q_p - q_p^d \qquad \lambda = \mathrm{diag}(\lambda_1, \lambda_2, ..., \lambda_n), \lambda_i > 0 \end{aligned} \tag{3}$$

Using the linearity of the parameters and definition of v in Eq. (3), the left hand side of Eq. (1) can be written as

$$M_p(q_p)\ddot{q}_p + C_p(q_p, \dot{q}_p)\dot{q}_p + g_p(q_p) = Y(q_p, \dot{q}_p, v, \dot{v})p \tag{4}$$

where $Y(q_p, \dot{q}_p, v, \dot{v}) \in \Re^{n \times r}$ is an acceleration-free controller regressor; n is the number of prosthetic degrees of freedom; $p \in \Re^{r \times 1}$ is a parameter vector.

The following control law is used to smooth control signal chattering, providing robustness to parameter uncertainties and unmodeled dynamics [19]:

$$\begin{aligned} u_p &= \hat{M}_p\dot{v} + \hat{C}_p v + \hat{g}_p - K_d\,\mathrm{sat}\,(s/\mathrm{diag}(\phi)) \\ &= Y(q_p, \dot{q}_p, v, \dot{v})\hat{p} - K_d\,\mathrm{sat}\,(s/\mathrm{diag}(\phi)) \end{aligned} \tag{5}$$

where $\hat{M}_p$, $\hat{C}_p$, and $\hat{g}_p$ are estimates of M_p, C_p, and g_p respectively; $K_d = \mathrm{diag}(K_{d1}, K_{d2}, ..., K_{dn}), K_{di} > 0$; ϕ is the width of the saturation function such that $\phi = \mathrm{diag}(\phi_1, \phi_2, ..., \phi_n), \phi_i > 0$. The addition of $\mathrm{sat}\,(s/\mathrm{diag}(\phi))$ in the above control law results in smoother control behavior in the boundary layer $|s| \leq \mathrm{diag}(\phi)$. Note that the division and saturation operations for s and $\mathrm{diag}(\phi)$ in the term $\mathrm{sat}\,(s/\mathrm{diag}(\phi))$ are interpreted element-wise and $\mathrm{diag}(\phi)$ is an n-element vector. Substituting the control law of Eq. (5) into Eq. (1) and using Eq. (3) yields the following error dynamics:

$$\dot{s} = -M_p^{-1}\left(C_p s + K_d\,\mathrm{sat}(s/\mathrm{diag}(\phi)) + M_p^{-1}Y(q_p, \dot{q}_p, v, \dot{v})\tilde{p}\right. \tag{6}$$

where $\tilde{p} = \hat{p} - p$ is parameter estimation error.

Using the control law of Eq. (5), it can be shown that all error trajectories starting outside the boundary layer will be attracted by the layer while those which start inside the boundary layer will remain inside for all $t \geq 0$ (the boundary layer is an invariant set). For this purpose, a boundary layer trajectory is defined to measure the distance between the current s to the boundary layer and also to trade off between tracking accuracy and robustness to unmodeled dynamics [18]:

$$s_\vartriangle = \begin{cases} 0 & \text{if } |s| \leq \mathrm{diag}(\phi) \\ s - \phi\,\mathrm{sat}\,(s/\mathrm{diag}(\phi)) & \text{if } |s| > \mathrm{diag}(\phi) \end{cases} \tag{7}$$

where $s_\vartriangle$ is an n-element vector; ϕ is the boundary layer thickness. The proposed control structure also satisfies the following reaching condition:

$$\frac{d}{dt}V(s_\vartriangle) \leq -\max(\gamma_i)\|s_\vartriangle\|_1 \tag{8}$$

where $\gamma = (\gamma_1, \gamma_2, ..., \gamma_n)$, $\gamma_i > 0$. To prove stability of the proposed controller, a scalar positive definite continuously-differentiable Lyapunov function is considered, which is a function of $s_\vartriangle$.

$$V(s_\vartriangle) = \frac{1}{2}\left(s_\vartriangle^T M_p s_\vartriangle\right) \tag{9}$$

Theorem 1: *Assume that $Y(q_p, \dot{q}_p, v, \dot{v})\tilde{p} \leq F$ and define $F_m = \max(F_i)$, $\gamma_m = \max(\gamma_i)$, and κ as a positive scalar. Given the Lyapunov function $V(s_\vartriangle)$ of Eq. (9) and the RS controller of Eq. (5), if $K_{d_i} \geq F_m + \gamma_m - \kappa\dot{q}_{p_{max}}\phi_i$, then $\dot{V}(s_\vartriangle) \to 0$ and $s_\vartriangle \to 0$ as $t \to \infty$ for all $p \in \Re^r$ and $s(0) \in \Re^n$, which implies $|s_i| \leq \phi_i$ and $e \leq \phi_i/\lambda_i$.*

Proof: Taking the derivative of Eq. (9), noting that $\dot{s}_\vartriangle = \dot{s}$ if starting outside the boundary layer, and substituting the error dynamics of Eq. (6) into Eq. (9) gives

$$\begin{aligned} \dot{V}(s_\vartriangle) = &-s_\vartriangle^T C_p s + \frac{1}{2}\left(s_\vartriangle^T \dot{M}_p s_\vartriangle\right) \\ &- s_\vartriangle^T K_d\,\mathrm{sat}\,(s/\mathrm{diag}(\phi)) + s_\vartriangle^T Y(q_p, \dot{q}_p, v, \dot{v})\tilde{p} \end{aligned} \tag{10}$$

Substituting $s = s_\vartriangle + \phi\,\mathrm{sat}\,(s/\mathrm{diag}(\phi))$ from Eq. (7) into Eq. (10) if starting outside the boundary layer, and using the skew symmetric property $\left(s_\vartriangle^T(\dot{M}_p - 2C_p)s_\vartriangle = 0\right)$ yields [20], [21]:

$$\dot{V}(s_\vartriangle) = -s_\vartriangle^T(C_p\phi + K_d)\mathrm{sat}\,(s/\mathrm{diag}(\phi)) + s_\vartriangle^T Y(q_p, \dot{q}_p, v, \dot{v})\tilde{p} \tag{11}$$

Tuning K_d and ϕ so $C_p\phi + K_d \geq K_m I$ (K_m is a positive scalar), and noting that $s_\vartriangle^T\mathrm{sat}\,(s/\mathrm{diag}(\phi)) = \|s_\vartriangle\|_1$ gives

$$\dot{V}(s_\vartriangle) \leq -K_m\|s_\vartriangle\|_1 + s_\vartriangle^T Y(q_p, \dot{q}_p, v, \dot{v})\tilde{p} \tag{12}$$

Defining $K_m = F_m + \gamma_m$, where $K_m = \max(K_{di})$ and noting that $s_\vartriangle^T F$ is upper bounded by $F_m\|s_\vartriangle\|_1$ yields

$$\dot{V}(s_\vartriangle) \leq -\gamma_m\|s_\vartriangle\|_1 \tag{13}$$

Therefore, if error trajectories start outside the boundary layer, $\dot{V}(s_\vartriangle) \to 0 \Rightarrow s_\vartriangle \to 0$ in a finite time less than $s_i(0)/\gamma_i$. In turn, the distance between s and the boundary layer approaches zero, showing that s is attracted by the boundary layer. This result implies that $|s_i| \leq \phi_i$ and $e \leq \phi_i/\lambda_i$ proving stability of the prosthesis / RS controller combination and boundedness of the tracking error trajectories by the boundary layer (regardless of starting point). It should also be noted that since C_p is upper bounded by $\kappa\|\dot{q}_p\|$ and $\|\dot{q}_p\| \leq \dot{q}_{p_{max}}$, such that $K_{d_i} \geq K_m - \kappa\dot{q}_{p_{max}}\phi_i$, $\dot{V}(s_\vartriangle) \to 0$ as $t \to \infty$. □

B. Robust Passivity Controller (RP)

With the definition of error and signal vectors from Eq. (3) and acceleration-free controller regressor from Eq. (4), the robust passivity-based control law is presented as [22]:

$$u_p = Y(q_p, \dot{q}_p, v, \dot{v})\hat{p} - K_d s \tag{14}$$

Substituting Eqs. (3) and (14) into Eq. (1), and defining $\hat{p} = p_0 + u_b$ and $\tilde{p} = p_0 - p$ yields the error dynamics

$$\dot{s} = -M_p^{-1}\left(C_p s + K_d s\right) + M_p^{-1} Y(q_p, \dot{q}_p, v, \dot{v})(\tilde{p} + u_b) \tag{15}$$

where p_0 is the nominal parameter vector, $\|\tilde{p}\| \leq \rho$, $\rho \geq 0$, and auxiliary control term u_b can be defined as [22]

$$u_b = \begin{cases} -\rho r/\|r\| & \text{, if } \|r\| > \epsilon \\ -\rho r/\epsilon & \text{, if } \|r\| \leq \epsilon \end{cases} \tag{16}$$

where $r = Y^T(q_p, \dot{q}_p, v, \dot{v})s$. Consider the following scalar positive definite Lyapunov function as a function of s:

$$V(s,e) = \frac{1}{2}\left(s^T M_p s + e^T \lambda K_d e\right) \tag{17}$$

Theorem 2: *Let $Q = \mathrm{diag}(\lambda^T K_d \lambda, K_d)$. Given the Lyapunov function $V(s,e)$ of Eq. (17), the RP controller of Eq. (14), and the auxiliary control term u_b of Eq. (16), if $\|r\| > \epsilon$, or $\|r\| \leq \epsilon$ and the error term has the property that $\|e\| \geq \sqrt{\rho\epsilon/2\lambda_{\min}(Q)}$, then $\dot{V}(s,e) \to 0$ as $t \to \infty$ for all $\tilde{p} \in \Re^r$, which implies boundedness of all tracking error trajectories.*

Proof: Taking the derivative of Eq. (17), substituting the error dynamics of Eq. (15), and using the skew symmetric property $\left(s^T(\dot{M}_p - 2C_p)s = 0\right)$ gives

$$\dot{V}(s,e) = s^T Y(q_p, \dot{q}_p, v, \dot{v})(\tilde{p} + u_b) - e^T \lambda^T K_d \lambda e - \dot{e}^T K_d \dot{e} \tag{18}$$

Using the definition of r yields

$$\dot{V}(s,e) = r^T(\tilde{p} + u_b) - e^T Q e \tag{19}$$

If $\|r\| > \epsilon$, $\quad u_b = -\rho r/\|r\|$

$$\dot{V}(s,e) \leq \|r\|\tilde{p} - \rho\|r\| - e^T Q e \tag{20}$$

and it can be concluded that $\dot{V}(s,e) < 0$ using the Cauchy-Schwartz inequality $(\|r\|(\tilde{p} - p) \leq 0)$. On the other hand, if $\|r\| \leq \epsilon$, then $u_b = -\rho r/\epsilon$ and

$$\dot{V}(s,e) \leq \|r\|\tilde{p} - \rho\|r\|^2/\epsilon - e^T Q e \tag{21}$$

Noting that $\|r\|\tilde{p} - \rho\|r\|^2/\epsilon$ is upper bounded by $\rho\epsilon/2$, $\dot{V}(s,e) < 0$ if

$$e^T Q e > \rho\epsilon/2 \tag{22}$$

As $e^T Q e$ is upper bounded by $\lambda_{\max}(Q)\|e\|^2$ and lower bounded by $\lambda_{\min}(Q)\|e\|^2$, the condition of Eq. (22) can be rewritten as

$$\|e\| \geq \sqrt{\frac{\rho\epsilon}{2\lambda_{\min}(Q)}} \tag{23}$$

Therefore, using the control law of Eq. (14), the term $r^T(\tilde{p}+u_b)$ in Eq. (19) is forced to be non-negative, regardless of the lack of information about $\tilde{p}$, which results in $\dot{V}(s,e) < 0$. That is, the prosthesis / RP controller emulates humanlike walking with the bounded tracking error trajectories. □

IV. PROSTHESIS CONTROL SIMULATIONS

In this section, the effectiveness of the proposed RS and RP controllers is demonstrated by performing simulation studies on the combined human-prosthesis model, while supplying the controllers with only the prosthesis model information from Section II. The proposed controllers of Section III are used to control the transfemoral prosthesis shown in Fig. 1 (i.e., prosthetic knee joint), and the rest of the joints are controlled by the feedback linearization human-inspired controller [17]. The RS and RP controllers are then compared to each other with regard to tracking performance in stance and non-stance phases for 40 steps.

The reference gait is obtained from the optimization problem in Section II, yielding desired trajectories y_d, q_c^d, and q_p^d for the controllers. It is assumed that both human and prosthetic parameters are unknown to the controller, the prosthetic ankle is underactuated, and the healthy ankle can be actuated by the amputee.

Fig. 2 shows tracking performances of the prosthetic knee during swing and stance phases for the RS and RP controllers. It can be seen that both controllers track the desired trajectories in both stance and non-stance phase. While the healthy human walking gait demonstrates roughly equal stance and swing phase durations, differences can arise from inherent asymmetries in the hybrid system. As mentioned in Section II, the human ankle remains actuated and able to inject energy into the system during human stance, while the passive prosthetic ankle is unable to do so. This discrepancy results in a shorter swing phase than in able-bodied walking (as shown in Fig. 2). Tracking for 40 steps yields $\mathrm{RMSE}_{\mathrm{RS}} = 0.0124$ rad and $\mathrm{RMSE}_{\mathrm{RP}} = 0.0064$ rad showing that in general, the RP controller outperforms the RS controller with regard to prosthetic knee angle tracking.

Fig. 3 show phase portraits of the stance and non-stance knee joints for the RS and RP controllers over 40 steps. The resulting portraits demonstrate convergence to a stable periodic orbit while applying a feedback linearization human-inspired controller to the able-bodied side.

V. EXPERIMENTAL IMPLEMENTATION AND RESULTS

A. AMPRO3 Implementation

In this section, the RS and RP controllers are implemented experimentally on the powered custom-built self-contained transfemoral prosthesis AMPRO3, as shown in Fig. 4a [23]. This device can be actuated at both knee and ankle joints

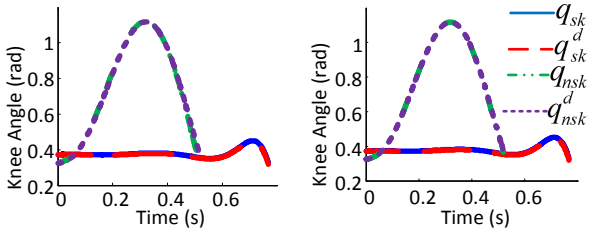

(a) RS controller (b) RP controller

Fig. 2: Tracking performance of the knee joint for the RS and RP controllers. q_{sk} is the knee angle during stance, and q_{nks} is the knee angle during swing (non-stance)

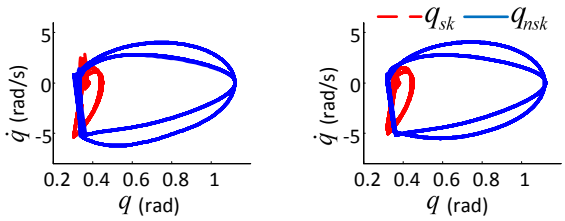

(a) RS controller (b) RP controller

Fig. 3: Phase portrait of the knee joint over 40 steps for both controllers

in the sagittal plane with a pair of torsion springs between the gearbox and joints, resulting in series elastic actuators (SEA). AMPRO3 also uses two relative incremental encoders at the knee and ankle joints. A 6-axis load cell is located right below the ankle joint to measure the ground reaction force (GRF), using the information to determine current gait state. An attached knee adaptor, or bypass, allows able-bodied human subjects to use the device for walking; see Fig. 4b. The scope of this study only aims to control the prosthesis knee joint, and as such, the prosthetic ankle is treated as a passive joint.

High-level controllers and trajectories are implemented in C++, organized as Robot Operating System (ROS) packages. A single BeagleBone Black (BBB) calculates trajectory and controller outputs at 200 Hz.

B. Experimental Results

In Section IV, the RS and RP controllers were validated in tracking and convergence of the limit cycle, and a comparison was performed. Now, the proposed controllers are tested on AMPRO3 with an able-bodied test subject. During the experiments, the prosthesis knee joint is controlled with the proposed RS and RP controllers, while the ankle behaves passively to emulate the point foot conditions used during simulation. A simple PD controller with small coefficients

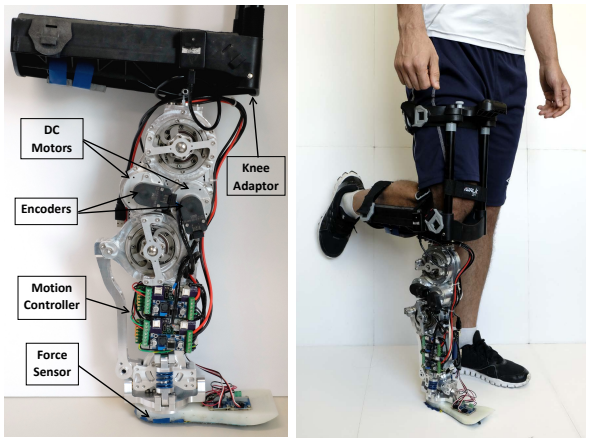

(a) (b)

Fig. 4: (a) AMPRO3 device, (b) Human test subject wearing AMPRO3

TABLE I: Experimental results of AMPRO3 using RS and RP controllers. Better values for each metric are underlined.

	RS	RP
$\tau_{\max}$ (N.m)	54	74
RMSE (rad)	0.0305	0.0221
$E_{\max}$ (rad)	0.1180	0.0785

for the ankle is employed with the goal of modeling the prosthetic ankle as a passive spring-damper mechanism (i.e., small rotation of the ankle).

For each controller, the healthy human test subject is instructed to walk for 2.5 min with the prosthesis at a treadmill speed of 2 mph. Fig. 5a and 5b show tracking performance of the RS and RP controllers respectively in a randomly selected time window $t \in [100, 104]$ sec. From Fig. 5, it is observed that both controllers achieve tracking of the prosthesis knee joint, providing a humanlike gait. However, the RP controller yields better knee angle tracking compared to the RS controller ($\text{RMSE}_{\text{RS}} = 0.0221$ rad versus $\text{RMSE}_{\text{RP}} = 0.0305$ rad) for 2.5 min of walking.

Fig. 6 demonstrates phase portraits of the prosthetic knee joint using RS and RP controllers for 2.5 min of walking. This figure shows a stable limit cycle of the prosthesis for both proposed controllers, indicating stable walking gaits.

Fig. 7 compares prosthetic knee torques for RS and RP controllers for $t \in [100, 104]$ sec. It can be seen that the RS controller generates fewer velocity sign changes during walking and lower peak torque values at the end of swing. These observations correlate with the test subject's perception of walking to be smoother and better while using the RS controller.

Table I lists maximum torque values $\tau_{\max}$, maximum tracking error $E_{\max}$, and RMSE for AMPRO3 using the proposed RS and RP controllers over 2.5 min of walking. Better values for each metric are underlined in the table, demonstrating that the RS controller decreases maximum prosthetic knee torque by 27% compared to RP controller, whereas the RP controller reduces maximum knee tracking error by 33% and improves RMSE by 27% compared to the RS controller.

To show humanlike walking for both proposed controllers, AMPRO3 walking results using the proposed RS and RP controllers in this paper can be seen in a video available at [24].

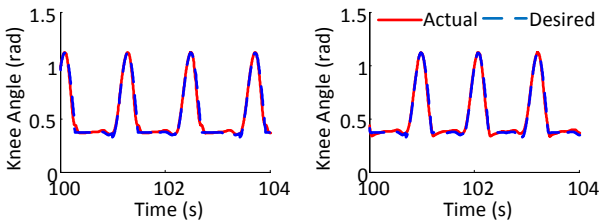

(a) RS controller (b) RP controller

Fig. 5: Experimental tracking performance of the prosthetic knee joint using different controllers

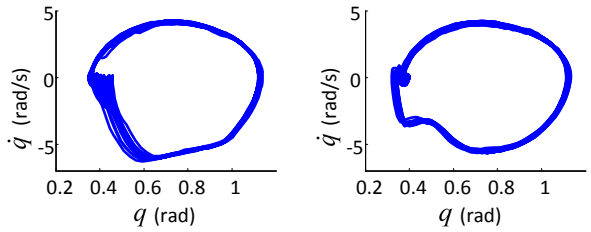

(a) RS controller (b) RP controller

Fig. 6: Experimental phase portrait of the prosthetic knee joint for 2.5 min of walking with different controllers

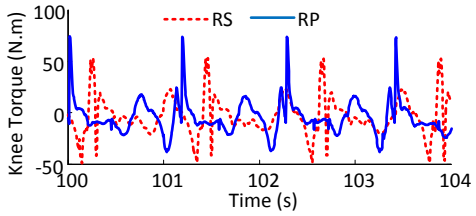

Fig. 7: Experimental prosthetic knee torque comparison between RS and RP controller. The two control signals are not in phase because they were recorded during two separate experiments.

VI. CONCLUSIONS AND FUTURE WORK

This paper presented, compared, and experimentally tested two robust model-based controllers, RS and RP, for the newly designed powered transfemoral prosthesis AMPRO3. Compared to traditional impedance controllers, there were no concerns regarding correct step cycle division and tedious parameter tuning. Stability and robustness of the proposed controllers were evaluated mathematically and via simulation.

Simulations on the human-prosthesis model (with the assumption of underactuated prosthetic ankle) for the proposed controllers showed that both controllers provided good prosthetic knee tracking performance, limit cycle convergence, and humanlike walking. Both proposed controllers were experimentally verified on AMPRO3 (with passive ankle) using an able-bodied human test subject, again yielding good tracking and reasonable prosthetic knee torque. From both simulation and experimental results, it was found that the RS controller rendered smoother walking and lower absolute peak torque compared to the RP controller. Conversely, the RP controller provided better tracking for the prosthetic knee joint.

In terms of future work, other adaptive and robust adaptive control paradigms in addition to the RS and RP controllers will be applied to the powered prosthesis AMPRO3 and compared with two commonly-used controllers: variable impedance and PD. There are also open questions related to the energy cost, subjective perception of walking quality, and robustness of fully actuated prosthetic walking with both RS and RP controllers.

REFERENCES

[1] T. Dillingham *et al.*, "Limb amputation and limb deficiency: epidemiology and recent trends in the United States," *Southern Medical Journal*, vol. 95, no. 8, pp. 875–884, 2002.

[2] D. A. Winter, *The Biomechanics and Motor Control of Human Gait: Normal, Elderly, and Pathological*. University of Waterloo Press, 1991.

[3] R. D. Gregg and J. W. Sensinger, "Towards biomimetic virtual constraint control of a powered prosthetic leg," *IEEE Transactions on Control Systems Technology*, vol. 22, no. 1, pp. 246–254, 2014.

[4] K. Fite, J. Mitchell, F. Sup, and M. Goldfarb, "Design and control of an electrically powered knee prosthesis," in *IEEE International Conference on Rehabilitation Robotics*, (Noordwijk), 2007.

[5] F. Sup, A. Bohara, and M. Goldfarb, "Design and control of a powered transfemoral prosthesis," *International Journal of Robotics Research*, vol. 27, no. 2, pp. 263–273, 2008.

[6] N. Fey, A. Simon, A. Young, and L. Hargrove, "Controlling knee swing initiation and ankle plantarflexion with an active prosthesis on level and inclined surfaces at variable walking speeds," *IEEE Journal of Translational Engineering in Health and Medicine*, vol. 2, pp. 1–12, 2014.

[7] S. Au, M. Berniker, and H. Herr, "Powered ankle-foot prosthesis to assist level-ground and stair-descent gaits," *Journal of Surgical Orthopedic Advances*, vol. 21, no. 4, pp. 654–666, 2008.

[8] C. G. Atkeson and S. Schaal, "Robot learning from demonstration," *International Conference on Machine Learning*, vol. 97, pp. 12–20, 1997.

[9] J. Nakanishi *et al.*, "Learning from demonstration and adaptation of biped locomotion," *Robotics and Autonomous Systems*, vol. 47, no. 2, pp. 79–91, 2004.

[10] A. M. Simon *et al.*, "Configuring a powered knee and ankle prosthesis for transfemoral amputees within five specific ambulation modes," *PLoS One*, vol. 9, no. 6, p. e99387, 2014.

[11] H. Zhao, S. Kolathaya, and A. D. Ames, "Quadratic programming and impedance control for transfemoral prosthesis," in *IEEE International Conference on Robotics and Automation*, (Hong Kong, China), 2014.

[12] H. Zhao, J. Horn, J. Reher, V. Paredes, and A. D. Ames, "First steps toward translating robotic walking to prostheses: a nonlinear optimization based control approach," *Autonomous Robots*, vol. 19, no. 1, pp. 1–18, 2011.

[13] Q. Nguyen and K. Sreenath, "l_1 adaptive control for bipedal robots with control Lyapunov function based quadratic programs," in *American Control Conference*, (Chicago, IL), 2015.

[14] S. C. Hsu, X. Xu, and A. D. Ames, "Control barrier function based quadratic programs with application to bipedal robotic walking," in *American Control Conference*, (Chicago, IL), 2015.

[15] M. Sharifi, S. Behzadipour, and G. Vossoughi, "Nonlinear model reference adaptive impedance control for humanrobot interactions," *Control Engineering Practice*, vol. 32, no. 8, pp. 9–27, 2014.

[16] A. D. Ames, "Human-inspired control of bipedal walking robots," *IEEE Transactions on Automatic Control*, vol. 59, no. 5, pp. 1115–1130, 2014.

[17] A. D. Ames, "First steps toward automatically generating bipedal robotic walking from human data," *Robotic Motion and Control*, vol. 422, 2011.

[18] J.-J. E. Slotine and J. A. Coetsee, "Adaptive sliding controller synthesis for non-linear systems," *International Journal of Control*, vol. 43, no. 6, pp. 1631–1651, 1984.

[19] J.-J. E. Slotine and W. Li, *Applied Nonlinear Control*. Prentice-Hall, 1991.

[20] V. Azimi, D. Simon, and H. Richter, "Stable robust adaptive impedance control of a prosthetic leg," in *Proceedings of the ASME Dynamic Systems and Control Conference*, (Columbus, OH), 2015.

[21] V. Azimi, D. Simon, H. Richter, and S. A. Fakoorian, "Robust composite adaptive transfemoral prosthesis control with non-scalar boundary layer trajectories," in *Proceedings of the American Control Conference*, (Boston, MA), 2016.

[22] M. Spong, S. Hutchinson, and M. Vidyasagar, *Robot Modeling and Control*. Wiley, 2005.

[23] H. Zhao, A. Hereid, E. Ambrose, and A. D. Ames, "3D multi-contact gait design for prostheses: hybrid system models, virtual constraints and two-step direct collocation," in *Conference on Decision and Control*, (Las Vegas, NV), 2016.

[24] V. Azimi, "Experimental and simulation results of AMPRO3 walking," https://www.youtube.com/watch?v=Aq8_H_nSAxI, accessed Feb. 16, 217.